J Mol Model (2013) 19:215–226
DOI 10.1007/s00894-012-1534-9

ORIGINAL PAPER

Density functional study on the adsorption of the drug isoniazid onto pristine and B-doped single wall carbon nanotubes

Nabanita Saikia · Ramesh C. Deka

Received: 31 May 2012 / Accepted: 9 July 2012 / Published online: 3 August 2012

Abstract The current study explores a new strategy to incorporate single wall carbon nanotubes (SWNTs)/doped SWNTs as carrier modules in target-specific administration of antitubercular chemotherapeutics through covalent and noncovalent functionalization onto the nanotube sidewall. Density functional studies illustrate that noncovalent functionalization of isoniazid (INH) is preferred over covalent attachment, exhibiting low adsorption energy values, HOMO–LUMO gap and comparison of quantum molecular descriptors performed in (5,5) and (9,0) SWNT systems. Substitution doping of boron facilitates the adsorption of INH onto the otherwise inert nanotube. Frontier orbital analysis reveals reorientation of electronic charge in the nanotubes after functionalization, the effect being more pronounced in the case of doped nanotubes. The charge transfer is significant in covalent functionalization of INH via the B-dopant atom, whereas in noncovalent functionalization a small amount of charge transfer is noted. Solvation studies demonstrate the dissolution of INH in B-doped (5,5) and (9,0) SWNTs to be higher compared to pristine nanotube-INH complexes. Functionalization of nanotubes via covalent and noncovalent means can foster pioneering prospects especially for experimental studies in this area of research.

Keywords Isoniazid · Carbon nanotube · Functionalization · Density functional theory · Reactivity descriptor

N. Saikia · R. C. Deka (✉)
Department of Chemical Sciences, Tezpur University,
Napaam,
Tezpur 784028 Assam, India
e-mail: ramesh@tezu.ernet.in

Introduction

Carbon nanotubes (CNTs), with their unique physiochemical properties, have made rapid advancements in nanotechnology, encompassing broad and diverse areas of application of which the use of CNTs as nanocarriers in drug delivery is an emergent topic. The nanodimension of CNT in addition to its unique electronic structure (resembling that of a rolled up graphene sheet) makes this class of nanomaterial highly unusual in its electronic properties [1] with applications in catalysis [2], storage devices [3] gas sensors [4] nanoelectronics [5] field effect transistors (FET) devices [6] and biosensors [7]. Much attention, at both the experimental and theoretical levels, has focused on the possibility of adsorption of polymers, proteins, peptides, and DNA onto the nanotube sidewall without drastically perturbing its electronic structure [8, 9]. The interaction of CNT with organic, aromatic molecules through covalent and noncovalent functionalization has attracted particular interest—the major motivation being to enhance its low solubility and dispersability in both organic and aqueous solvents [10–12]. Some of the methods commonly used to functionalize single wall carbon nanotubes (SWNT) involve hydrogenation [13], ozonization [14], fluorination [15], 1,3-dipolar cycloaddition [16], attachment of bioconjugate polymers, biomolecules like peptides, nucleic acids, therapeutic agents etc. [17, 18]. Aromatic compounds undergo weak interaction (physisorption) with the SWNT sidewall through noncovalent functionalization, which modifies nanotube electronic and transport properties to an extent [19, 20]. The $\pi - \pi$ stacking interactions attributable to intermolecular forces between the reacting groups are responsible for interlayer bonding; in turn leading to nanotube solubility in organic solvents [21]. For this reason, noncovalent functionalization via π – stacking or van der Waals interaction is a hot area of research [22–24]. On the other hand, chemical functionalization involving attachment of functional units to

nanotube sidewalls through covalent bonds modifies not only the physical and chemical properties of the nanotube but expands its scope of application. Substitution doping of CNT carbon atoms with boron/nitrogen atoms is the most effective way to regulate nanotube electronic structure and chemical reactivity as it introduces chemically active sites into the otherwise inert tube. The boron/nitrogen doping of CNT at very low concentration introduces impurity states below the conduction band (above the valence band) of semiconducting nanotubes and below (above) the first van Hove singularity above (below) the Fermi level in the metallic nanotubes [25]. The boron atom can be used as the site for adsorption of therapeutic as well as aromatic molecules in such a way as to functionalize the CNT. Substitution doping in particular can influence the intermolecular interactions and covalent functionalization of nanotubes [26, 27]. There have been extensive theoretical [28–30] and experimental [31–33] studies on B-doped CNTs, suggesting that substitution doping can change the physical and chemical properties of nanotubes.

Exploitation of CNT in drug delivery has made great advancements in recent years, with extensive studies on the use of CNT as a carrier module for cancer chemotherapeutics [34, 35] in addition to addressing the toxicity issues both in vivo and in vitro [36]. With expansion into domains of application other than cancer chemotherapy, through covalent functionalization, CNTs have been tailored with anti-inflammatory drugs such as nimesulide [37] and nifedipine [38], and antitubercular drugs like isoniazid (INH) [39] pyrazinamide [40] and 2-methylheptylisonicotinate (MHI) (an analogue of isoniazid) [41], which represent the most potent and widely used drugs for the treatment of tuberculosis.

INH is a widely used, potent antitubercular drug effective against strains of *Mycobacterium tuberculosis*, working in combination with pyrazinamide and rifampicin. Although INH has been in use for the treatment of tuberculosis since 1950, the exact mechanism of drug action is not completely understood. INH is a prodrug that is activated by *M. tuberculosis* catalase peroxidase enzyme (KatG) [42, 43] and interferes with the biosynthesis of the mycolic acid that constitutes the fatty acid component of the mycobacterial cell wall. Studies have shown that isonicotinoyl radical—the activated form of INH—reacts with β-nicotinamide adenine dinucleotide (NAD^+/NADH), the cofactor of long-chain 2-trans-enoyl-acyl carrier protein reductase InhA [44–46], which is the key enzyme involved in the biosynthesis of long chain fatty acids and mycolic acids [47, 48]. KatG catalyzes the conversion of Mn^{II} to Mn^{III}, and the Mn^{III} ion facilitates in the oxidation of INH [49]. Incorporation of CNT as a carrier module for INH facilitates target-specific drug loading and delivery at the active binding site and prevents the premature degradation of drug molecules upon administration within the body. For effectual drug delivery pursuits, the adsorption, distribution, metabolism, excretion, and toxicity of CNT are highly dependent on the extent of functionalization, coating and length of the nanotube [50].

The objective of the present study was to perform density functional theory (DFT) calculations to investigate the interaction of INH with pristine and B-doped CNT through covalent and non-covalent functionalization. We addressed the following issues: (1) the stable geometry and adsorption energies for covalent and noncovalent interaction of INH onto pristine/B-doped SWNT sidewalls; (2) modulation in electronic properties of pristine nanotube in addition to the effect of B-doping on adsorption of drug molecule in terms of variation in HOMO–LUMO energy gap, and global reactivity descriptors; (3) frontier orbital contribution to the electronic charge distribution in the drug-nanotube system, (4) charge transfer between INH and B-doped CNT through covalent and non-covalent functionalization; and finally (5) solubility of INH-nanotube conjugate in aqueous media, which can provide a general insight into its biocompatibility.

Computational procedure

The electronic structure calculations were performed with the program DMol^3, which uses an all-electron linear combination of the atomic orbital density functional theory (DFT) approach. The gas phase calculations were performed on INH, a pristine armchair (5,5) SWNT comprising four unit cells (10.465 Å), and a zigzag (9,0) SWNT comprising three unit cells (13.549 Å) with the ends terminated by hydrogen atoms (to saturate the dangling hydrogen bonds and also a means of functionalization). The substitution doping of pristine (5,5) and (9,0) SWNTs was done by replacing one carbon atom of CNT with a boron dopant atom. During geometry optimization of pristine/B-doped nanotubes and the corresponding INH-pristine/B-doped system, all the atoms were allowed to relax. The double numerical basis set with polarization function (DNP), equivalent to 6–31 G** basis set of Gaussian basis set, and the PW91 exchange correlation functional within the generalized gradient approximation (GGA) were used. The Fukui indices were calculated for the INH drug molecule to determine electrophilic as well as nucleophilic sites preferred for covalent and noncovalent functionalization.

For adsorption of INH onto (5,5) and (9,0) SWNT sidewalls by non-covalent interaction, both parallel and perpendicular orientations of INH were considered. The covalent attachment of INH onto the two nanotube sidewalls was facilitated by the boron dopant atom (reactive adsorption site) with elimination of one hydrogen atom from the amine group of INH. The adsorption energy of INH onto pristine/B-doped (5,5) and (9,0) SWNTs via noncovalent functionalization and covalent linkage were calculated using the

following equations:

$$E_{ads} = \left(E_{INH} + E_{SWNT/B-doped\ SWNT}\right)) - E_{total} \quad (1)$$

where E_{INH} is the total energy of INH, $E_{SWNT/B\text{-}doped\ SWNT}$ is the total energy of SWNT/B-doped SWNT and E_{total} is the total energy of the system.

For noncovalent functionalization, the E_{ads} is defined as-

$$E_{ads} = \left(E_{INH(deprotonated)} + E_{B-doped\ SWNT}\right) - E_{total} \quad (2)$$

where $E_{INH(deprotonated)}$ is the total energy of deprotonated INH, $E_{B\text{-}doped\ SWNT}$ is the total energy of B-doped (5,5) and (9,0) SWNTs and E_{total} is the total energy of the system for covalent functionalization.

DFT is constructive in explaining the chemical reactivity, stability and site selectivity of complex systems that make use of quantum molecular descriptors like global hardness (η), chemical potential (μ) and electrophilicity indices (ω), which carry information about the reactivity of molecules helpful to interpreting its properties and to understanding the global nature of molecules in terms of their stability. The concept of electronegativity put forward by Pauling [51] is defined as "*the power of an atom in a molecule to attract electrons towards itself*". The higher the electronegativity of the species, the greater its electron accepting power or, rather, electrophilicity. On the other hand, the concept of hardness first formulated by Pearson [52, 53] states "*hard like hard and soft like soft*", which forms the basis of the popular HSAB theory.

In an N-electron system with total energy (E) and external potential [$\upsilon(\vec{r})$], the electronegativity (χ) is given by:

$$x = -\left(\frac{\delta E}{\delta N}\right)_{\upsilon(\vec{r})} = -\mu \quad (3)$$

where μ is defined as the negative of electronegativity. The η is expressed in terms of second derivative of energy with respect to the external potential [$\upsilon(\vec{r})$] and is given by:

$$\eta = \frac{1}{2}\left(\frac{\delta^2 E}{\delta N^2}\right)_{\upsilon(\vec{r})} \quad (4)$$

According to Mulliken [54], the working equations for μ and η using the finite difference method are given by:

$$\mu = -\chi = -\frac{1}{2}(I + A) \quad (5)$$

and

$$\eta = \frac{1}{2}(I - A) \quad (6)$$

where I is the ionization potential and A the electron affinity of the molecule.

The electrophilicity index defined by Parr [55] is given as:

$$\omega = \frac{\mu^2}{2\eta} \quad (7)$$

The electrophilicity index is a measure of electrophilicity of an electrophile; the higher the electrophilicity of a molecule, the greater its electrophilic character.

The solvation energies of functionalized INH-pristine/B-doped (5,5) and (9,0) SWNTs were obtained by single point calculations on the optimized geometries in the presence of water (dielectric constant ε=78.54) with the help of "Conductor like Screening Model" (COSMO) implemented in DMol^3. The difference in energies between the gas phase and solvent phase geometries yielded Gibb's free energy of solvation. The dielectric solvation energies for the adsorbed complexes were also computed and compared for covalent and noncovalent functionalization.

Results and discussion

Structure and electronic properties of isoniazid, pristine and B-doped nanotubes

The optimized geometries of INH, pristine and B-doped (5,5) and (9,0) SWNTs are depicted in Fig. 1. INH is a non-planar molecule with the amine group protruding out of the molecular plane as shown in Fig. 1a. The calculated bond lengths and bond angles are in good agreement with reported X-ray crystallographic data [56]. The C–C bond lengths in pristine (5,5) and (9,0) SWNTs are calculated to be 1.42 Å, which corresponds to sp^2 hybridization and is concurrent with the experimental value of 1.44 Å [57]. Boron doping in (5,5) SWNT suggests an increase in C–B bond length to 1.514 Å, whereas in (9,0) SWNT it increases to 1.517 Å with the boron atom protruding out of the nanotube framework. Thus, to an extent, doping breaks the delocalized network of pristine nanotube, with a loss of symmetry at the site of substitution.

Noncovalent functionalization of pristine and B-doped nanotube with the IHN drug molecule

Structure and energetics

Two possible modes of noncovalent interaction of INH onto pristine and B-doped (5,5) and (9,0) SWNTs were investigated, i.e., with parallel and perpendicular orientations of adsorption onto the tube sidewall. The orientation of adsorption of INH for both pristine and B-doped CNTs is

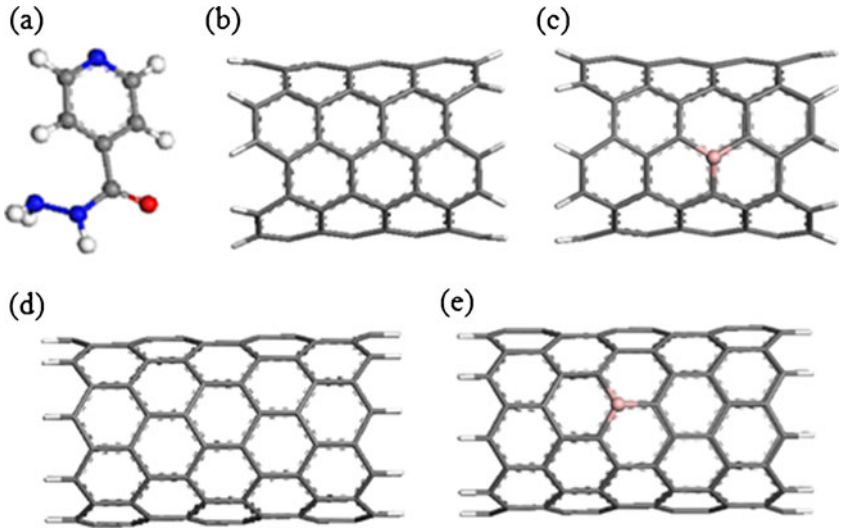

Fig. 1 Optimized geometries of **a** isoniazid (INH), **b** pristine (5,5) single wall carbon nanotube (SWNT), **c** boron (B)-doped (5,5) SWNT, **d** pristine (9,0) carbon nanotube (CNT), **e** B-doped (9,0) CNT

illustrated in Fig. 2. In parallel adsorption of INH onto pristine and doped (5,5) and (9,0) SWNTs, noncovalent functionalization is manifested through delocalized $\pi - \pi$ stacking between the aromatic rings of the nanotube and the pyrazine ring of INH in addition to interaction with amine groups and oxygen atoms of INH. For the parallel interaction of INH onto pristine (5,5) and (9,0) nanotubes, INH prefers to become adsorbed at the hollow site in order to maximize the $\pi - \pi$ interaction (Fig. 2b, h). The equilibrium distance of interaction of INH with pristine and doped CNT, along with the adsorption energy values are provided in Table 1. In INH/(5,5) SWNT, the parallel orientation is preferred over the perpendicular conformation due to enhanced $\pi - \pi$ stacking interaction, where the amine group of INH is in close proximity to the nanotube sidewall. In doped nanotubes, however, the adsorption is quite different as described in Fig. 2. In doped (5,5) and (9,0) SWNTs, INH slips out from the hollow site (Fig. 2d, j), which is indicative of the boron atom influencing adsorption at the hollow site. The adsorption energy is lower in the INH-(9,0) SWNT system (Table 1), with the parallel orientation for adsorption exhibiting a higher adsorption energy value compared to perpendicular adsorption. The equilibrium distance of interaction (Table 1) is lower in (5,5) SWNT compared to (9,0) nanotubes, which may be due to the difference in chirality of the two nanotubes. Unlike pristine nanotube, doping leads to

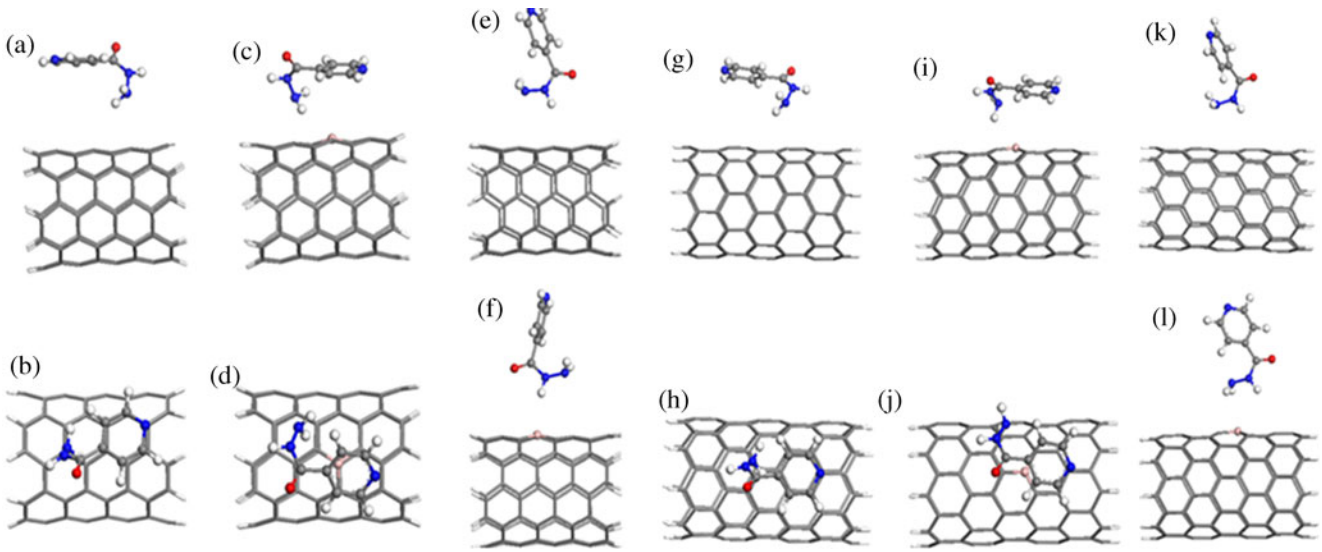

Fig. 2a–l Noncovalent adsorption of INH onto pristine and B-doped (5,5) and (9,0) SWNTs. **a** Side view of INH adsorbed onto pristine (5,5) SWNT at hollow site (parallel orientation).; **b** front view. **c** Side view of INH adsorbed onto B-doped (5,5) SWNT at slipped hollow site (parallel orientation).; **d** front view. **e** Perpendicular adsorption of INH onto pristine (5,5) SWNT. **f** Perpendicular adsorption of INH onto B-doped (5,5) SWNT. **g** Side view of INH adsorbed onto pristine (9,0) SWNT at hollow site (parallel orientation); **h** front view. **i** Side view of INH adsorbed onto B-doped (9,0) SWNT at slipped hollow site (parallel orientation; **j** front view. **k** Perpendicular adsorption of INH onto pristine (9,0) SWNT. **l** Perpendicular adsorption of INH onto B-doped (9,0) SWNT

Table 1 Optimum distance of interaction, adsorption energy, HOMO – LUMO energy gap and global reactivity descriptors of the antitubercular drug isoniazid (INH), pristine and boron (B)-doped (5,5) and (9,0) single wall carbon nanotubes (SWNTs) along with their complexes with INH

System	Optimum distance of interaction (Å)	Adsorption energy (eV)	HOMO – LUMO gap (eV)	η (eV)	μ (eV)	ω (eV)
Isoniazid	-	-	3.476	1.738	-4.177	4.876
(5,5) SWNT	-	-	0.941	0.470	-3.776	15.156
B-doped (5,5) SWNT	-	-	0.777	0.388	-3.815	18.736
INH-(5,5) SWNT (parallel)	2.981	0.0889	0.856	0.428	-3.863	17.433
INH-(5,5) SWNT (perpendicular)	2.844	0.0883	0.859	0.429	-3.819	16.983
INH-B doped (5,5) SWNT (parallel)	2.529	0.7104	0.770	0.385	-3.895	19.703
INH-B doped (5,5) SWNT (perpendicular)	2.689	0.6104	0.773	0.386	-3.842	19.101
(9,0) SWNT	-	-	0.617	0.308	-4.269	29.544
B doped (9,0) SWNT	-	-	0.379	0.189	-4.338	49.664
INH-(9,0) SWNT (parallel)	3.067	0.0727	0.620	0.310	-4.327	30.198
INH-(9,0) SWNT (perpendicular)	3.038	0.0640	0.614	0.307	-4.306	30.198
INH-B doped (9,0) SWNT (parallel)	2.694	0.2527	0.381	0.190	-4.379	50.341
INH-B doped (9,0) SWNT (perpendicular)	2.900	0.3278	0.406	0.203	-4.481	49.456

an enhancement in adsorption energy values (Table 1). Following a trend similar to that observed in pristine nanotube, adsorption of INH onto (5,5) SWNT (parallel orientation) is stronger compared to (9,0) SWNT at the optimum interacting distance. The introduction of boron dopant influences adsorption of INH in the otherwise inert nanotube, leading to enhancement of adsorption energy values for both nanotubes, as doping perturbs the electronic structure and properties of the pristine nanotube by breaking the sp^2 delocalized network of electrons. The observed low values of adsorption energy for both pristine and doped nanotubes is in agreement with weak adsorption (physisorption) coming into play.

Comparison of HOMO–LUMO difference and quantum molecular descriptors

The variation in the HOMO–LUMO energy gap, quantum molecular descriptors for INH, pristine and B-doped (5,5) and (9,0) SWNTs along with the functionalized units were calculated and compared (Table 1). Gas phase calculations on INH suggest it to be a very stable molecule with a high HOMO–LUMO gap of 3.476 eV. On the other hand, in pristine (5,5) and (9,0) SWNTs, (9,0) CNT is found to be more reactive, demonstrating an energy difference of 0.617 eV compared to (5,5) CNT with a HOMO–LUMO energy gap of 0.941 eV. Substitution doping with boron results in further lowering of the energy gap of both nanotubes (Table 1) with B-doped (9,0) SWNT being more reactive than B-doped (5,5) SWNT. The η value [which correlates to the reactivity (stability) of the system] in B-doped (9,0) SWNT is higher than B-doped (5,5) SWNT, suggesting the (9,0) nanotube to be more reactive (less stable) compared to the (5,5) nanotube. On the other hand, doping enhances the reactivity of the otherwise stable (inert) pristine nanotube. In INH adsorbed onto pristine and doped (5,5) CNTs, the change in η value is not very significant, as observed in the (9,0) CNT system. Upon functionalization of the two nanotubes, the chemical stability of INH/nanotube is lowered, i.e., its reactivity increases. The chemical potential (μ) of the B-doped INH-SWNT complex is higher than that of the (5,5) CNT-INH system for both pristine and doped nanotubes. On the other hand, for covalent functionalization, in the INH-(5,5) CNT system, the μ value is higher than the noncovalent functionalization. However, in the (9,0) CNT-INH system, the μ value for covalent functionalization is lower than that for noncovalent functionalization. The ω value in (9,0) SWNT (pristine and B-doped) is high compared to (5,5) CNT. The high ω value of the (9,0) SWNT system suggests that it behaves more as an electrophile compared to (5,5) SWNT. Noncovalent functionalization results in an increase in ω values for both systems, but in the INH-(9,0) SWNT system the values were found to be quite high.

The adsorption of pyrazinamide (PZA) onto pristine (5,5) CNT leads to further lowering of the HOMO – LUMO energy gap (0.856 eV) for both the parallel and perpendicular (0.859 eV) orientations; with the variation in energy gap being comparable. The η value follows a similar trend as it decreases with adsorption of INH onto (5,5) SWNT. Adsorption of INH onto pristine (9,0) SWNT results in an increase of HOMO – LUMO energy gap, and η value. For INH/B-doped (5,5) and (9,0) CNT systems, the variations in the HOMO – LUMO energy gap, and η value are not very prominent compared to doped nanotube without functionalization. Thus we can say that noncovalent functionalization of INH does not modify drastically the electronic states of doped (5,5) and (9,0) SWNTs. The same conclusion also holds for

pristine nanotubes, wherein the weak physisorption of INH onto the nanotube sidewall does not cause significant modulation in energy gap or reactivity descriptor values.

Frontier orbital analysis in INH, pristine and doped nanotubes

Frontier orbital analysis has been quite instrumental in determining the charge localization/delocalization in a molecule, based on which we can have a qualitative overview of the electronic charge distribution in a molecule. The Frontier orbital approach as proposed by Koopmans' theorem [58, 59] for closed shell systems is very appropriate for explaining the stability and chemical reactivity of molecules based on HOMO and LUMO orbitals. The energy corresponding to HOMO represents the ionization potential of the molecule, while that of the LUMO represents the corresponding electron affinity. Using Koopmans' theorem, I and A values can be correlated with Frontier orbitals via the relationship:

$$I = -E_{\mathrm{HOMO}} \text{ and } A = -E_{\mathrm{LUMO}}$$

Localization of electron density in HOMO advocates a particular site to be nucleophilic whereas the site where LUMO is localized is electrophilic in nature. A high HOMO–LUMO energy gap indicates greater stability and low reactivity of the chemical system. The HOMO and LUMO orbitals of INH, pristine and B-doped (5,5) are illustrated in Fig. 3, and the HOMO and LUMO plots for the corresponding (9,0) SWNTs are given in Fig. 4. Since INH is a partially delocalized system due to the presence of the aromatic pyrazine ring, the HOMO and LUMO plots show charge delocalization throughout the molecule (Fig. 3a, b) with contributions on the electronegative nitrogen and oxygen atoms. In pristine (5,5) SWNT, the HOMO (Fig. 3c) is delocalized uniformly throughout the nanotube sidewall along the C–C bonds perpendicular to tube axis, whereas the LUMO is delocalized along the C-C bonds parallel to the nanotube axis (Fig. 3d). In B-doped (5,5) CNT, the HOMO (although delocalized throughout the nanotube sidewall) becomes reoriented around the boron atom (Fig. 3e), which exhibits the major charge contribution. The LUMO, on the other hand, remains unperturbed (Fig. 3f) with less electron contribution from the boron atom.

Moving to pristine (9,0) CNT, the HOMO is delocalized throughout the nanotube sidewall (Fig. 4a) at alternate rings, whereas the LUMO is highly localized along the tube edges with no contribution to the sidewall (Fig. 4b), which suggests that the edges of the (9,0) SWNT are more reactive compared to the sidewall. For B-doped (9,0) CNT, the charge contribution from HOMO becomes reoriented (Fig. 4c), with the major contribution being on the boron atom, whereas the LUMO is localized along one of the tube edges with no distribution towards the other end (Fig. 4d). Thus doping of pristine (9,0) SWNT brings about significant modification in the charge distribution of the two nanotubes.

Frontier orbital analysis in functionalized nanotubes interacting with isoniazid

The influence of the boron dopant atom on the charge contribution from HOMO and LUMO for the adsorption

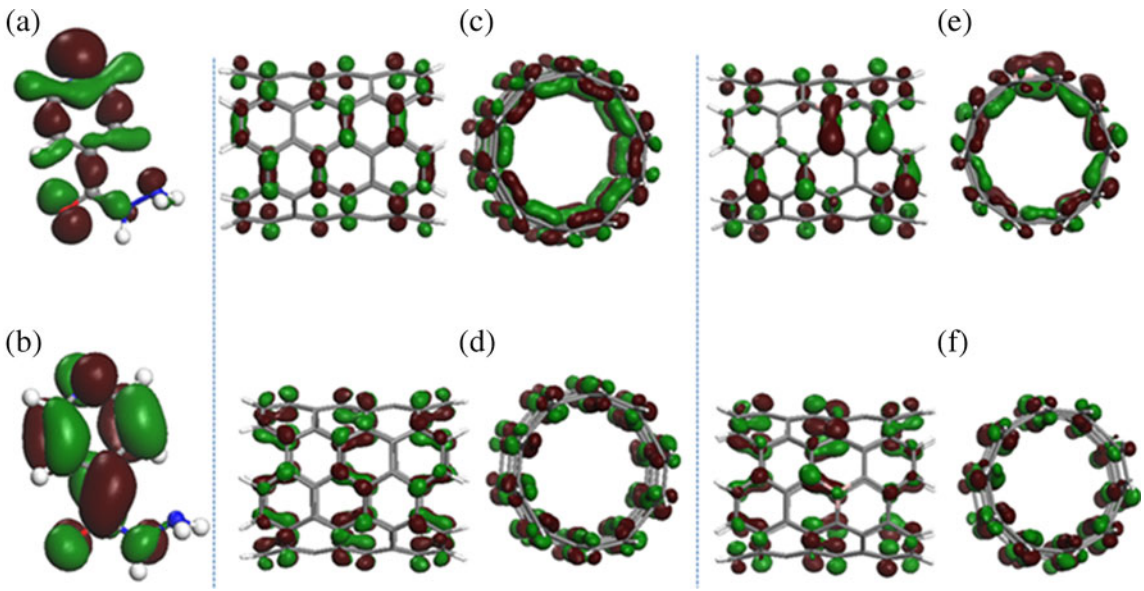

Fig. 3 **a** HOMO of INH. **b** LUMO of INH. **c** Side and front view depiction of HOMO in pristine (5,5) SWNT. **d** Side and front view depiction of LUMO in pristine (5,5) SWNT. **e** Side and front view depiction of HOMO in B-doped (5,5) SWNT. **f** Side and front view depiction of LUMO in B-doped (5,5) SWNT

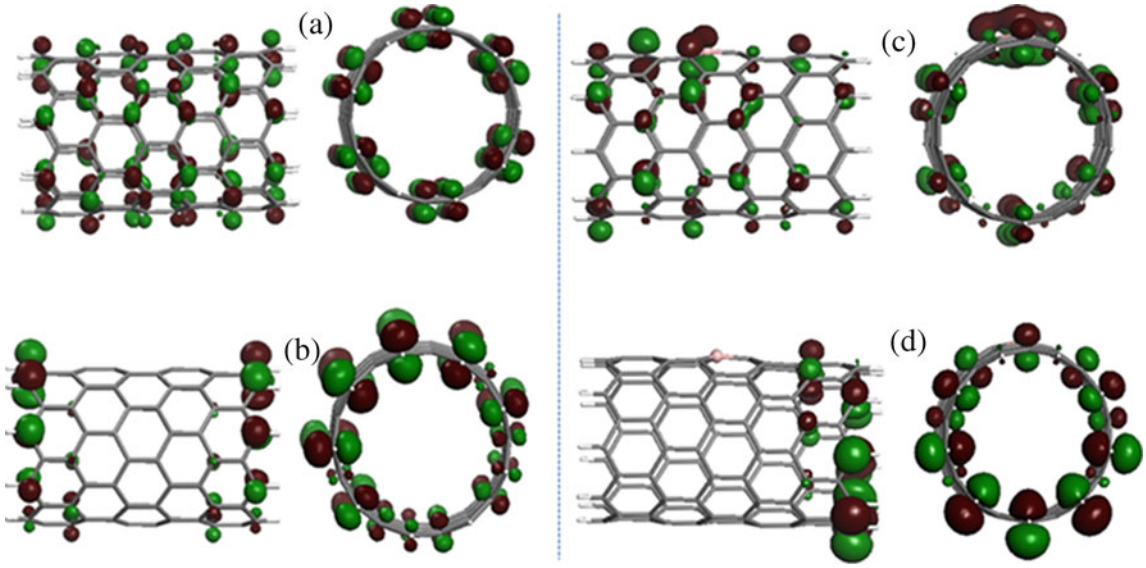

Fig. 4 **a** Side and front view depiction of HOMO in pristine (9,0) SWNT. **b** Side and front view depiction of LUMO in pristine (9,0) SWNT. **c** Side and front view depiction of HOMO in B-doped (9,0) SWNT. **d** Side and front view depiction of LUMO in B-doped (9,0) SWNT

of INH onto (5,5) and (9,0) SWNTs is rather interesting as illustrated in Figs. 5 and 6, respectively. If we observe the adsorption of INH onto pristine (5,5) SWNT (parallel and perpendicular orientation) at the optimum distance of interaction, the adsorbed INH molecule does not bring about any major perturbation in the electronic charge distribution of the nanotube (Fig. 5a–d). This is suggestive of the fact that weak adsorption (physisorption) of INH through noncovalent functionalization does not initiate any major perturbation in the otherwise inert nanotube. The same conclusion cannot be drawn for the INH/(9,0) SWNT system. For the parallel adsorption of INH onto (9,0) SWNT, the HOMO (Fig. 6a) resembles that of a pristine (9,0) SWNT without any doping whereas LUMO exhibits a charge reorientation (Fig. 6b) along the nanotube edges. In the perpendicular adsorption of INH, the trend in HOMO remains same but LUMO is localized along one of the tube edges with no contribution at the other end (Fig. 6c, d). The modulation in HOMO and LUMO orbitals after functionalization is more prominent in pristine (9,0) CNT compared to (5,5) CNT.

In the case of doped (5,5) and (9,0) SWNTs, the physisorption of INH shows prominent changes in HOMO and LUMO. For INH/B-doped (5,5) SWNT, the frontier orbital analysis was carried out for both the

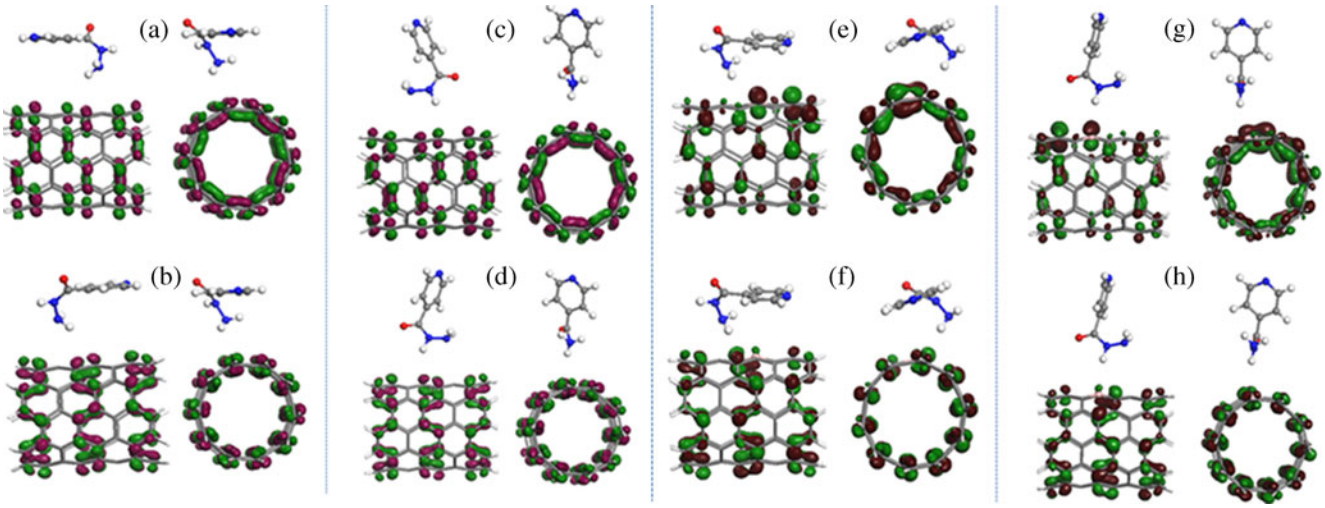

Fig. 5 **a** Side and front view depiction of HOMO in parallel adsorption of INH onto (5,5) SWNT. **b** The corresponding LUMO plot depicting the side and front views. **c** Side and front view depiction of HOMO in perpendicular adsorption of INH onto (5,5) SWNT; **d** LUMO plot depicting the side and front views. **e** Side and front view depiction of HOMO in parallel adsorption of INH onto B-doped (5,5) SWNT; **f** LUMO plot depicting the side and front views. **g** Side and front view depiction of HOMO in perpendicular adsorption of INH onto (5,5) SWNT; **h** LUMO plot depicting the side and front views

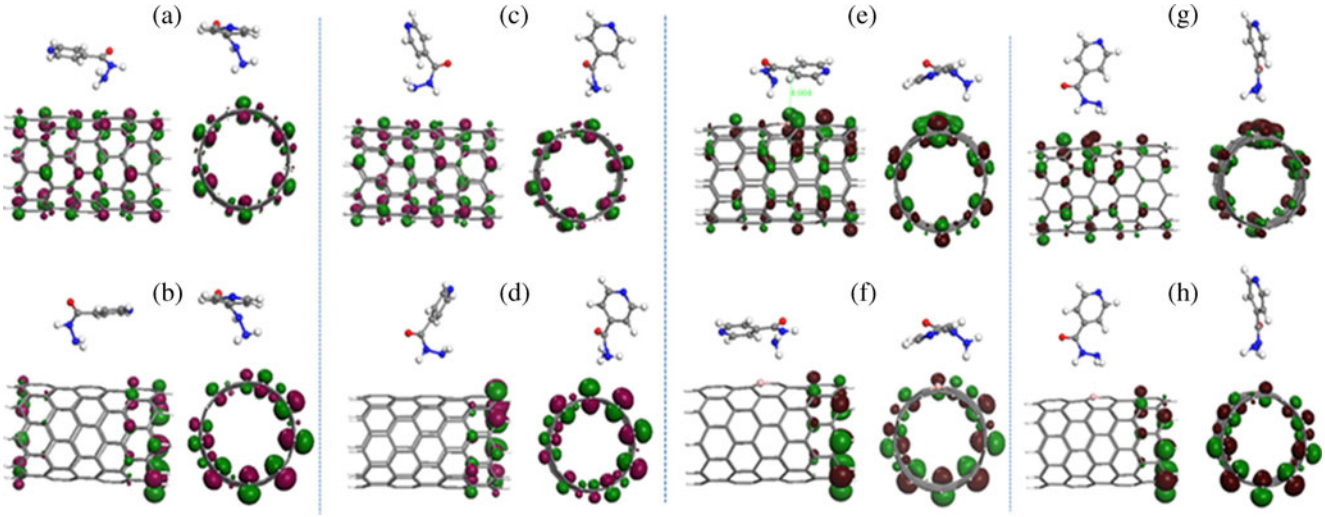

Fig. 6 **a** Side and front view depiction of HOMO in parallel adsorption of INH onto (9,0) SWNT; **b** corresponding LUMO plot depicting the side and front views. **c** Side and front view depiction of HOMO in perpendicular adsorption of INH onto (9,0) SWNT; **d** corresponding LUMO plot depicting the side and front views. **e** Side and front view depiction of HOMO in parallel adsorption of INH onto B-doped (9,0) SWNT; **f** the corresponding LUMO plot depicting the side and front views. **g** Side and front view depiction of HOMO in perpendicular adsorption of INH onto (9,0) SWNT; **h** corresponding LUMO plot depicting the side and front views

parallel and perpendicular orientations. In the parallel conformation, the presence of the boron dopant atom influences the adsorption of INH. The HOMO, although delocalized along the tube sidewall, makes a major contribution to boron and the adjoining carbon atoms of the tube in close proximity to the pyrazine ring of the isoniazid molecule (Fig. 5e). The trend in LUMO remains unperturbed, like that of the pristine nanotube, but with a charge deficiency on the boron atom (Fig. 5f). The perpendicular adsorption of INH also shows a similar trend in HOMO charge distribution whereas the LUMO remains delocalized throughout the tube sidewall, with a charge deficiency on the boron atom (Fig. 5g, h). The LUMO becomes localized along one of the tube edges facing towards the amine group of INH similar to that in B-doped (9,0) CNT (Fig. 4d). For the perpendicular conformation, the HOMO displays a major charge contribution on the boron atom with the LUMO remaining mostly unperturbed.

The HOMO and LUMO isosurface thus provide a qualitative overview of the charge contribution in pristine and functionalized (5,5) and (9,0) SWNTs with INH, and how the substitution doping of nanotubes with boron atoms affects the adsorption of INH in the otherwise inert nanotube. The absence of any charge distribution from the isoniazid molecule for the noncovalent adsorption onto (5,5) and (9,0) SWNTs illustrates that the physisorption is governed basically by the properties of the nanotube electronics rather than that of the drug molecule, and the conformational framework of the drug molecule remains unperturbed.

Covalent adsorption of isoniazid onto B-doped (5,5) and (9,0) nanotubes

Structure and energetics

The optimized geometries of the covalent functionalization of isoniazid onto B-doped (5,5) and (9,0) SWNTs via the boron dopant atom are illustrated in Fig. 7. The covalent attachment of isoniazid onto pristine (5,5) and (9,0) SWNTs were not studied here as it is rather difficult to determine the selectivity for bonding onto the sidewall of pristine (5,5) and (9,0) nanotubes with an all C backbone. The equilibrium bond distance between the B–N atoms at the site of covalent attachment, adsorption energies, HOMO–LUMO energy gap and quantum molecular descriptors are detailed in Table 2.

The covalent bonding of INH onto the B-doped nanotube is achieved via the nitrogen atom of the amine group of INH (with loss of the hydrogen atom) and the boron atom of the nanotube, which constitute the site of covalent attachment. The B–N bond protrudes out of the molecular plane as observed in Fig. 7. The covalent functionalization of INH onto the B-doped nanotube further perturbs the sp^2 symmetry of the nanotube (as doping of the boron atom to an extent breaks the symmetry of the carbon network). The adsorption energy of isoniazid onto B-doped (5,5) CNT is higher (1.517 eV) than B-doped (9,0) CNT at an adsorption energy value of 0.995 eV, which suggests IHN is adsorbed strongly onto doped (5,5) CNT rather than the (9,0) tube at the covalent bonding distance.

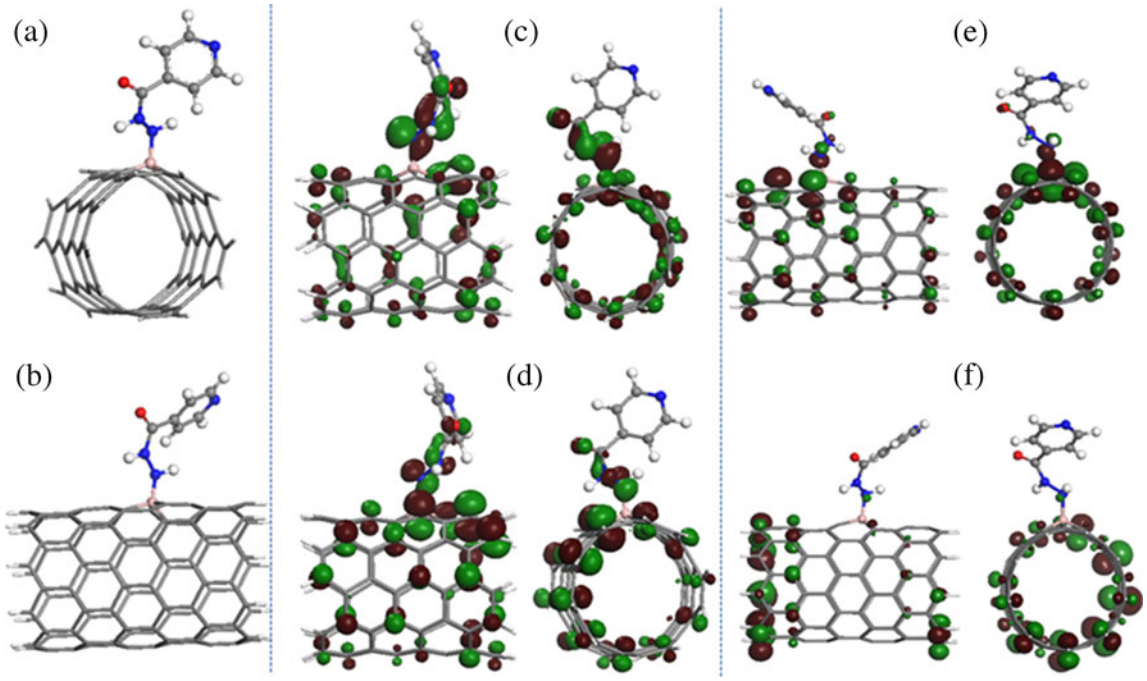

Fig. 7a–f Covalent functionalization of INH onto doped (5,5) and (9,0) SWNTs. **a** INH adsorbed onto B-doped (5,5) CNT. **b** INH adsorbed onto B-doped (9,0) SWNT. **c** Front and side view depiction of HOMO in INH-B-doped (5,5) SWNT; **d** corresponding LUMO plot. **e** Front and side views of HOMO in INH adsorbed onto B-doped (9,0) SWNT; **f** corresponding LUMO plot

Quantum molecular descriptors and HOMO-LUMO energy difference

The HOMO – LUMO energy gap in INH-B-doped (9,0) CNT system is ten times lower than that of the INH-B-doped (5,5) CNT system as observed in Table 2. The adsorption energy values associated with covalent functionalization are high compared to those of noncovalent functionalization, but the system becomes highly unstable as observed from the decreased HOMO–LUMO energy gap and η values. Thus, covalent functionalization breaks the symmetry as well as the stability of the molecule. Nevertheless, for covalent functionalization there is significant increase in ω values: (9,0) SWNT demonstrates a six-fold increase, whereas in the (5,5) CNT system the ω value is nearly doubled.

Frontier orbital analysis

The frontier orbital contribution to HOMO and LUMO in INH-B-doped (5,5) and (9,0) SWNTs (Fig. 7) exemplifies significant delocalization and charge transfer between the CNT sidewall and the amine group of INH via the boron dopant atom, with the covalently bonded INH reorienting most of the charge distribution towards itself. Covalent functionalization leads to significant perturbation of the charge distribution of the nanotube, modulating the frontier orbitals around the site of functionalization. In the covalent functionalization of isoniazid onto B-doped (9,0) CNT, reorientation of the frontier orbital contribution from the HOMO is noted (Fig. 7e), with the charge delocalized around the functional unit of the otherwise inert nanotube. Similarly, in

Table 2 Optimum distance of interaction, adsorption energy, HOMO–LUMO energy gap and comparison of the global reactivity descriptors in deprotonated INH, and INH adsorbed onto B-doped (5,5) and (9,0) SWNTs

System	Optimum distance of interaction (Å)	Adsorption energy (eV)	HOMO – LUMO gap (eV)	η (eV)	μ (eV)	ω (eV)
Isoniazid (deprotonated)			1.926	0.963	-3.667	6.982
INH-B doped (5,5) SWNT	1.598	1.157	0.558	0.279	-4.321	33.461
INH-B doped (9,0) SWNT	1.585	0.995	0.059	0.029	-4.222	302.195

the INH-B-doped (9,0) SWNT system, the dissolution or solubility is higher for parallel adsorption compared to perpendicular orientation (−1.553 eV).

The LUMO on the other hand remains localized around the nanotube edges, making no major contribution to the sidewall (Fig. 7f). Thus, we can say that covalent functionalization perturbs the electron delocalized framework of the nanotube, exhibiting significant charge transfer between the two interacting units.

Mulliken charge analysis and charge transfer

In the INH-B-doped (5,5) CNT system, the charge on the boron atom in the B-doped nanotube is 0.145e. After the parallel adsorption of INH onto B-doped (5,5) CNT, the charge on the boron atom increases to 0.168e. However, for the perpendicular adsorption of INH, the charge on the B-atom reduces to 0.103e. The parallel adsorption of INH results in charge transfer from INH to the B-atom of the nanotube by 0.023e. Interestingly, for the covalent adsorption of INH, an enhancement of 0.303e in charge is observed on the boron atom. Covalent functionalization leads to enhanced charge transfer from INH to the boron atom of doped (5,5) CNT by 0.158e.

For the B-doped (9,0) CNT-INH system, the charge on the boron atom of (9,0) CNT is 0.135e, which is lower compared to the B-doped (5,5) CNT. Upon parallel adsorption of INH onto the nanotube sidewall, the charge on boron atom increases to 0.161e, which suggests a charge transfer from INH to the boron dopant atom. Likewise, for the perpendicular adsorption of INH, depletion of charge (0.091e) is observed on the boron atom. Covalent functionalization results in enhanced charge transfer from INH to the boron atom of the nanotube (charge on boron=0.293e). In both the B-doped (5,5) and (9,0) CNT/INH complexes, the covalent functionalization of INH leads to enhanced charge transfer from the INH drug molecule to the boron dopant atom of the nanotube.

Solvation studies using COSMO

The Gibbs free energy of solvation (solvation energy) helps in understanding the extent of solubility of a substance in any given solvent. Solvation studies were performed in aqueous media, water having a dielectric constant value of 78.54. Water was chosen as the solvent because water can easily mimic the biological environment of the body and aid in the understanding of the solvation process of the nanotube-conjugated drug molecule. Table 3 summarizes the Gibbs free energy and solvation energy values of INH drug adsorbed onto pristine and B-doped (5,5) and (9,0) SWNTs via covalent and noncovalent functionalization. The negative values of solvation energy observed point to the degree of dissolution as well as the thermodynamic spontaneity of the system. The doped nanotube-INH complex was found to be highly soluble in water compared to the pristine nanotube-INH complex. The enhanced solubility of the drug-nanotube complex in water illustrates it to be suitable for drug delivery applications, with the noncovalent functionalization having added advantages in terms of drug release and dissolution over the covalent functionalization, where breakage of the covalent bond is associated with high energy. Although toxicity studies on carbon nanotubes both in vivo and in vitro belongs to another completely different research domain, it does pose some limitations on DFT methodologies. Through solvation studies, we can have a generalized understanding of the solubility and dissolution of nanotube-conjugated drug molecules in aqueous media as a proxy for the biological environment of the body.

Table 3 Gibb's free energy and solvation energy values of INH adsorbed onto pristine and B-doped (5,5) and (9,0) SWNTs via covalent and noncovalent functionalization

System	Gibb's free energy (eV)	Dielectric solvation energy (eV)
INH-(5,5) SWNT (parallel)	-1.134	-1.399
INH-(5,5) SWNT (perpendicular)	-1.125	-1.413
INH-B doped (5,5) SWNT (parallel)	-1.166	-1.457
INH-B doped (5,5) SWNT (perpendicular)	-1.235	-1.584
INH-B doped (5,5) SWNT (covalent adsorption)	-1.081	-1.375
INH-(9,0) SWNT (parallel)	-1.106	-1.422
INH-(9,0) SWNT (perpendicular)	-1.087	-1.416
INH-B doped (9,0) SWNT (parallel)	-1.237	-1.665
INH-B doped (9,0) SWNT (perpendicular)	-1.168	-1.553
INH-B doped (9,0) SWNT (covalent adsorption)	-1.113	-1.551

Conclusions

We report the covalent and noncovalent functionalization of pristine and B-doped (5,5) and (9,0) SWNTs with the drug molecule INH using DFT. The chemical reactivity of pristine nanotube increases with substitution doping of boron atom; (9,0) SWNT being more reactive compared to (5,5) SWNT. Introduction of boron dopant into the otherwise inert nanotube facilitates the adsorption of INH as observed from the high adsorption energy values. The parallel adsorption of INH onto (5,5) SWNT is preferred, whereas in (9,0) the perpendicular adsorption is favoured over the parallel

adsorption of INH. Solvation studies using COSMO demonstrate the enhanced solubility of the drug-nanotube complex in aqueous media. Since noncovalent functionalization via $\pi - \pi$ stacking is weak compared to covalent functionalization, the solubility of the noncovalently bonded INH-SWNT complex is much higher in aqueous media. In summary, doping modulates the structure and electronic properties of pristine nanotube, and facilitates the adsorption of INH onto the nanotube sidewall. Unlike covalent functionalization, noncovalent functionalization does not perturb nanotube electronic properties drastically. Frontier orbital analysis shows that B-doping of pristine (5,5) and (9,0) CNTs leads to significant modulation of nanotube electronic charge distribution at the site of introduction of the dopant atom. On the other hand, substitution doping of nanotubes with boron atoms affects the adsorption of INH in the otherwise inert nanotube; for noncovalent functionalization the perturbation is not very marked, whereas for covalent functionalization the perturbation in electron delocalization within the nanotube exhibits significant charge transfer between the two interacting units. Mulliken charge population analysis on B-doped (5,5) and (9,0) CNT/INH complexes sees enhanced charge transfer from the INH drug molecule to the boron dopant atom of the nanotube. Functionalization of nanotubes with drug molecules enhance their solubility and biocompatibility thereby opening up potential applications in drug delivery.

Acknowledgments The authors thank the Department of Science and Technology (DST), New Delhi, India for funding, and providing necessary assistance for carrying out the project.

References

1. Dresselhaus MS, Dresselhaus G, Avouris P (2001) Carbon nanotubes: synthesis, structure. properties and applications. Springer, Berlin
2. Wu G, Chen YS, Xu BQ (2005) Remarkable support effect of SWNTs in Pt catalyst for methanol electrooxidation. Electrochem Commun 7:1237–1243
3. Dag S, Ozturk S, Ciraci S, Yildirim T (2005) Adsorption anddissociation of hydrogen molecules on bare and functionalized carbon nanotubes. Phys Rev B 72(155404):1–8
4. Kong J, Chapline MG, Dai H (2001) Functionalized carbon nanotubes for molecular hydrogen sensors. J Adv Mater 13:1384–1386
5. Collins PG, Arnold MS, Avouris P (2001) Engineering carbon nanotubes and nanotube circuits using electrical breakdown. Science 292:706–709
6. de Heer WA, Chatelain A, Ugarte D (1995) A carbon nanotube field-emission electron source. Science 270:1179–1180
7. Dong L, Fischer AB, Lu M, Martin MT, Moy D, Simpson D (1996) Reversible and irreversible immobilization of enzymes on graphite fibrils. J Mol Recognit 93:383–388
8. Hirsch A (2002) Functionalization of single-walled carbon nanotubes. Angew Chem 41:1853–1859
9. Chen RJ, Zhang Y, Wang D, Dai H (2001) Noncovalent sidewall functionalization of single-walled carbon nanotubes for protein immobilization. J Am Chem Soc 123:3838–3839
10. Lin Y, Taylor S, Li HP, Fernando KAS, Qu LW, Wang W, Gu LR, Zhou B, Sun YP (2004) Advances toward bioapplication of carbon nanotubes. J Mater Chem 14:527–541
11. Star A, Liu Y, Grant K, Ridvan L, Stoddart JF, Steuerman DW, Diehl MR, Boukai A, Heath JR (2003) Noncovalent side-wall functionalization of single-walled carbon nanotubes. Macromolecules 36:553–560
12. Lin Y, Allard LF, Sun YP (2004) Protein-affinity of single-walled carbon nanotubes in water. J Phys Chem B 108:3760–3764
13. Nikitin A, Ogasawara H, Mann D, Denecke R, Zhang Z, Dai H, Cho K, Nilsson A (2005) Hydrogenation of single-walled carbon nanotubes. Phys Rev Lett 95(1-4):225507
14. Banerjee S, Wong SS (2002) Rational sidewall functionalization and purification of single-walled carbon nanotubes by solution-phase ozonolysis. J Phys Chem B 106:12144–12151
15. Khabashesku VN, Billups WE, Margrave JL (2002) Fluorination of single-wall carbon nanotubes and subsequent derivatization reactions. Acc Chem Res 35:1087–1095
16. Georgikilas V, Tagmatarchis N, Pantaratto D, Bianco A, Briand JP, Prato M (2002) Amino acid functionalization of water soluble carbon nanotubes. Chem Commun 24:3050–3051
17. Liu Z, Cai W, He L, Nakayama N, Chen K, Sun X, Chen X, Dai H (2007) In vivo biodistribution and highly efficient tumour targeting of carbon nanotubes in mice. Nat Nanotechnol 2:47–52
18. Lacerda L, Bianco A, Prato M, Kostarelos K (2006) Carbon nanotubes as nanomedicines: from toxicology to pharmacology. Adv Drug Delivery Rev 58:1460–1470
19. Sumanasekera GU, Pradhan BK, Romero HE, Adu KW, Eklund PC (2002) Giant thermopower effects from molecular physisorption on carbon nanotubes. Phys Rev Lett 89(1-4):166801
20. Star A, Han TR, Gabriel JCP, Bradley K, Grŭner G (2003) Interaction of aromatic compounds with carbon nanotubes: correlation to the Hammett parameter of the substituent and measured carbon nanotube FET response. Nano Lett 3:1421–1423
21. Sun Y, Wilson SR, Schuster DI (2001) High dissolution and strong light emission of carbon nanotubes dissolved in aniline. J Am Chem Soc 123:5348–5349
22. Chen J, Liu H, Weimer WA, Halls MD, Waldeck DH, Walker GC (2002) Noncovalent engineering of carbon nanotube surfaces by rigid, functional conjugated polymers. J Am Chem Soc 124:9034–9035
23. Fagan SB, Santos EJG, Filho AGS, Filho JM, Fazzio A (2007) Ab initio study of double-wall carbon nanotubes under uniaxial pressure. Chem Phys Lett 437:79–82
24. Gotovac S, Honda H, Hattori Y, Takahashi K, Kanoh H, Kaneko K (2007) Effect of nanoscale curvature of single-walled carbon nanotubes on adsorption of polycyclic aromatic hydrocarbons. Nano Lett 7:583–587
25. Buonocore F (2007) Doping effects on metallic and semiconductor single-wall carbon nanotubes. Philos Mag 87:1097–1105
26. Collins PG, Bradley K, Ishigami M, Zettl A (2000) Extreme oxygen sensitivity of electronic properties of carbon nanotubes. Science 287:1801–1804
27. Zurek E, Pickard CJ, Autschbach J (2007) A density functional study of the ^{13}C NMR chemical shifts in functionalized single-walled carbon nanotubes. J Am Chem Soc 129:4430–4439
28. Katakoski J, Krasheninnikov AV, Ma Y, Foster AS, Nordlund K, Nieminen RMB (2005) B and N ion implantation into carbon nanotubes: insight from atomistic simulations. Phys Rev B 71(1-6):205408
29. Ponomarenko O, Radny MW, Smith PV (2006) Small-radius clean and metal-doped boron carbide nanotubes: a density functional study. Phys Rev B 74(1-10):125421

30. Yu SS, Zheng WT, Wen QB, Zheng B, Tian HW, Jiang Q (2006) Nature of substitutional impurity atom B/N in zigzag single-wall carbon nanotubes revealed by first-principle calculations. IEEE Trans Nanotechnol 5:595–598
31. Zhao J, Xi RH (2003) Electronic and photonic properties of doped carbon nanotubes. J Nanosci Nanotechnol 3:459–478
32. Caroll DL, Redlich P, Blaśe X, Charlier JC, Curran S, Ajayan PM, Roth S, Rühle M (1998) Effects of nanodomain formation on the electronic structure of doped carbon nanotubes. Phys Rev Lett 81:2332–2335
33. Hsu WK, Firth S, Redlich P, Terrones M, Terrones H, Zhu YQ, Grobert N, Schilder A, Clark RJH, Kroto HW, Walton DRM (2000) Boron doping effects in carbon nanotubes. J Mater Chem 10:1425–1429
34. Chen J, Chen S, Zhao X, Kuznetsova LV, Wong SS, Ojima I (2008) Functionalized single-walled carbon nanotubes as rationally designed vehicles for tumor-targeted drug delivery. J Am Chem Soc 130:16778–16785
35. Wu W, Li R, Bian X, Zhu Z, Ding D, Li X, Jia Z, Jiang X, Hu Y (2009) Covalently combining carbon nanotubes with anticancer agent: preparation and antitumor activity. ACS Nano 9:2740–2750
36. Cui HF, Vashist SK, Al-Rubeaan K, Luong JHT, Sheu FS (2010) Interfacing carbon nanotubes with living mammalian cells and cytotoxicity issues. Chem Res Toxicol 23:1131–1147
37. Zanella I, Fagan SB, Mota R, Fazzio A (2007) Ab initio study of pristine and Si-doped capped carbon nanotubes interacting with nimesulide molecules. Chem Phys Lett 439:348–353
38. Liu H, Bu Y, Mi Y, Wang Y (2009) Interaction site preference between carbon nanotube and nifedipine: a combined density functional theory and classical molecular dynamics study. J Mol Struct (THEOCHEM) 901:163–168
39. Gallo M, Favila A, Glossmam-Mitnik D (2007) DFT studies of functionalized carbon nanotubes and fullerenes as nanovectors for drug delivery of antitubercular compounds. Chem Phys Lett 447:105–109
40. Saikia N, Deka RC (2010) Theoretical study on pyrazinamide adsorption onto covalently functionalized (5,5) metallic single-walled carbon nanotube. Chem Phys Lett 500:65–70
41. Saikia N, Deka RC (2011) Density functional calculations on adsorption of 2-methylheptylisonicotinate antitubercular drug onto functionalized carbon nanotube. Comput Theor Chem 964:257–261
42. Johnsson K, Schultz PG (1994) Mechanistic studies of the oxidation of isoniazid by the catalase-peroxidase from *Mycobacterium tuberculosis*. J Am Chem Soc 116:7425–7426
43. Zhang Y, Heym B, Allen B, Young D, Cole S (1992) The catalase peroxidase gene and isoniazid resistance of *Mycobacterium tuberculosis*. Nature 358:591–593
44. Banerjee A, Dubnau E, Quémard A, Balasubramanian V, Um KS, Wilson T, Collins D, de Lisle G, Jacobs WR Jr (1994) InhA, a gene encoding a target for isoniazid and ethionamide in *Mycobacterium tuberculosis*. Science 263:227–230
45. Quémard A, Dessen A, Sugantino M, Jacobs WR, Sacchettini JC, Blanchard JS (1996) Binding of the catalase-peroxidase-activated isoniazid to wild-type and mutant *Mycobacterium tuberculosis* enoyl-ACP reductases. J Am Chem Soc 118:1561–1562
46. Nguyen M, Quemard A, Marrakchi H, Bernadou J, Meunier B (2001) The nonenzymatic activation of isoniazid by Mn^{III}-pyrophosphate in the presence of NADH produces the inhibition of the enoyl-ACP reductase InhA from Mycobacterium tuberculosis. C R Acad Sci Paris, Série IIc, Chimie: Chemistry 4:35–40
47. Daffé M, Draper P (1998) The envelope layers of mycobacteria with reference to their pathogenicity. Adv Microbiol Physiol 39:131–203
48. Marrakchi H, Laneelle G, Quémard A (2000) InhA, a target of the antituberculous drug isoniazid, is involved in a mycobacterial fatty acid elongation system. FAS-II Microbiology 146:289–296
49. Magliozzo RS, Marcinkeviciene JA (1997) The role of Mn(II)-peroxidase activity of mycobacterial catalase-peroxidase in activation of the antibiotic isoniazid. J Biol Chem 272:8867–8870
50. Helland A, Wick P, Koehler A, Schmid K, Som C (2007) Reviewing the environmental and human health knowledge base of carbon nanotubes. Environ Health Perspective 115:1125–1131
51. Pauling L (1960) The nature of chemical bond. Cornell University Press, Ithaca
52. Pearson RG (1963) Hard and soft acids and bases. J Am Chem Soc 85:3533–3543
53. Pearson RG (1997) Chemical hardness: applications from molecules to solids. Wiley-VCH, Weinheim
54. Mulliken RS (1934) Electronic structures of molecules. XI. Electroaffinity, molecular orbitals and dipole moments. J Chem Phys 2:782–793
55. Parr RG, von Szentpaly L, Liu S (1999) Electrophilicity index. J Am Chem Soc 121:1922–1924
56. Jensen LH (1954) The crystal structure of isonicotinic acid hydrazide. J Am Chem Soc 76:4663–4667
57. Saito R, Dresselhaus G, Dresselhaus MS (2001) Physical properties of carbon nanotubes. Imperial College Press, London
58. Koopmans T (1933) Ordering of wave functions and eigen energies to the individual electrons of an atom. Physica 1:104–113
59. Phillips JC (1961) Generalized Koopmans' theorem. Phys Rev 123:420–424